ELECTROSTATIC ADHESION FOR ADDED FUNCTIONALITY OF COMPOSITE STRUCTURES

Callum J. C. Heath, Ian P. Bond and Kevin D. Potter

Advanced Composites Centre for Innovation and Science (ACCIS),
Department of Aerospace Engineering, University of Bristol, Queen's Building,
University Walk, Bristol BS8 1TR, UNITED KINGDOM
Email: ch8193@bristol.ac.uk , web page: http://www.accismultifunctional.com/

Keywords: Electrostatic Adhesion, Composite, Functionality, Variable Stiffness

ABSTRACT

Electrostatic adhesion can be used as a means of reversible attachment. The incorporation of electrostatic adhesion into fibre reinforced polymer (FRP) composite structures could provide significant value added functionality. Imparting large potential differences (~ 2 kV) across electrodes generates an attractive force, thus providing a means of attachment. This could be used as a reversible latching mechanism or as a means of controllable internal connectivity. Varying the connectivity for discrete elements of a substructure of a given design allows for control of internal load paths and moment of area of the cross section. This could facilitate variable stiffness (both in bending and torsion). Using a combination of existing fabrication techniques, functional electrodes have been integrated within a FRP. Copper polyimide thin film laminate material has been both co-cured with carbon fibre reinforced epoxy (CFRP) and bonded to PVC closed cell foam core material to provide a range of structural configurations with integrated electrodes. The ability of such integrated devices to confer variations in global bending stiffness of basic beam structures is investigated. Through the application of 4 kV across integrated electrostatic adhesive devices, a 112% increase in flexural stiffness has been demonstrated for a composite sandwich structure.

1 INTRODUCTION

In recent years there has been a growing interest in multi-functionality of composite structures [1]. Ideally, the material and structure of fibre reinforced composites (FRPs) are produced simultaneously, thus allowing for functional integration at the earliest fabrication steps, fully integrating it into the host structure. Integration of conductive electrode elements allows exploitation of electrostatic adhesion to control the connectivity between discrete substructures. Reversible adhesion in this manner could provide controllable global bending stiffness, a potentially high value, additional structural functionality.

In this paper, a study is made of the use of electrostatic adhesion for controlled latching of both monolithic and sandwich configuration composite structures. The intention is to assess the achievable change in bending stiffness resulting from the application of electrostatic adhesion at the mid-plane in a variety of beams. Existing research in this field has, to the best of the authors' knowledge, only considered the use of electrostatic adhesion in this manner for thin plate structures in bending [2], and only for relatively low forces in sandwich structures [3]. This research aims to consider sandwich structures at higher levels of force to extend the use of such technology to a wider range of applications.

An assessment of the current use of electrostatic adhesion for variable stiffness in FRPs is included. An outline of the fabrication methods used for incorporation of the electrodes into composite sandwich structures is also provided. The fabrication process used has enabled the production of highly planar integrated electrode surfaces, with low surface roughness and waviness. The surface finish produced enables very close contact between inherently rigid structural elements, providing levels of electrostatic adhesive holding strength higher than an existing sandwich beam concept [3], and of similar magnitude to non-structurally integrated electrostatic adhesive elements [2]. A demonstration of the devices in three-point bend flexural tests, at order of magnitude higher loading conditions than previous tests of similar devices, shows the increased potential of the technology from the enhancements provided herein. The limitations and further research required for electrostatically induced variable stiffness are also considered.

2 BACKGROUND

Electrostatic adhesion is used here to define the attractive force generated between parallel plates at high potential difference. The configuration of the device is shown in Figure 1.

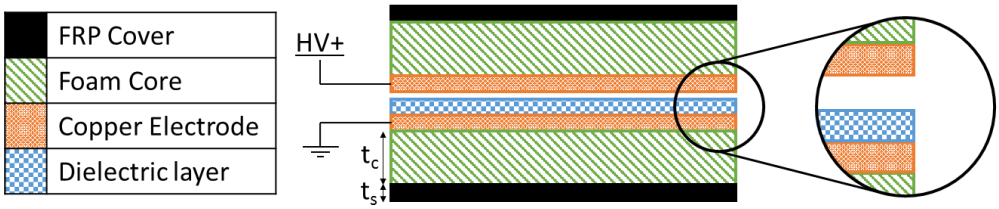

Figure 1: Basic electroadhesive sandwich device configuration t_c = Core thickness t_s = FRP skin thickness

2.1 Existing Literature

Kuder *et al* provide a relatively comprehensive review of variable stiffness technology for morphing applications [4]. This study considers the use of variable stiffness as a beneficial functionality in its own right, however, the aforementioned review highlighted the use of Electro-Bonded Laminate (EBL) technology for variable stiffness. Tabatha *et al* [5] presented a variable bending stiffness concept using thin polyimide layers between nickel electrodes. Voltage increases the observed friction between layers, thus increasing bending resistance. This concept was extended by Bergamini *et al* [3,6,7] who focused on replacing permanent adhesion between layers of a composite beam with reversible electrostatic bonding. The experimental methods therein incorporate a dielectric layer, such as polytetrafluoroethylene (PTFE), between stiffer layers, such as CFRP face sheets. Upon activation of an electric field, a normal holding force is generated, allowing for increased shear stress transfer between the layers as the electric field strength increases, thus increasing bending stiffness.

Whilst the use of electrostatic adhesion to integrate variable stiffness to composite structures is not a novel concept, there is a need for advancements of this technology in terms of achievable stiffness variation and fabrication improvement to facilitate wider applicability. Previously, EBL has been used for vibration suppression [6], with limited investigation into the use of variable stiffness as a function in its own right [2].

The use of EBL for control of internal connectivity has been considered for some adaptive twist concepts. Through controlling the connectivity of spar elements, one can open or close discrete bays of a larger section, thus controlling overall torsional stiffness [8,9]. Thoughtful integration of electrostatic adhesion within a sandwich structure could achieve controllable bending stiffness in a similar manner.

2.2 Structural Concept

Bergamini *et al* summarise the potential means of variable stiffness in a very succinct manner, with three key options: Change in Modulus, Change in Geometry, or Change in Topology [6]. Electrostatic adhesion of discrete elements of the substructure is a means of changing the topology. Considering a basic beam element (Figure 2 (b)), the introduction of a central split with no significant connectivity can drastically reduce the effective second moment of area. For a simple beam section (Figure 2 (a)) the second moment of area is given below (*b = width , d = thickness*).

$$I = \frac{bd^3}{12} \tag{1}$$

For the split beam, the depth of each is half of the complete beam, thus yielding a second moment of area as follows, with each section contributing half of the overall second moment of area (*I*).

$$I = 2\frac{b\left(\frac{d}{2}\right)^3}{12} = 2\frac{b\frac{d^3}{8}}{12} = \frac{2bd^3}{96}$$
$$I = \frac{bd^3}{48} \tag{2}$$

This represents a 75% reduction in bending stiffness if the Young's modulus of each section is equivalent. This effect can be amplified by means of multiple beam splits (Figure 2 (c)), thus the EBL concept [7].

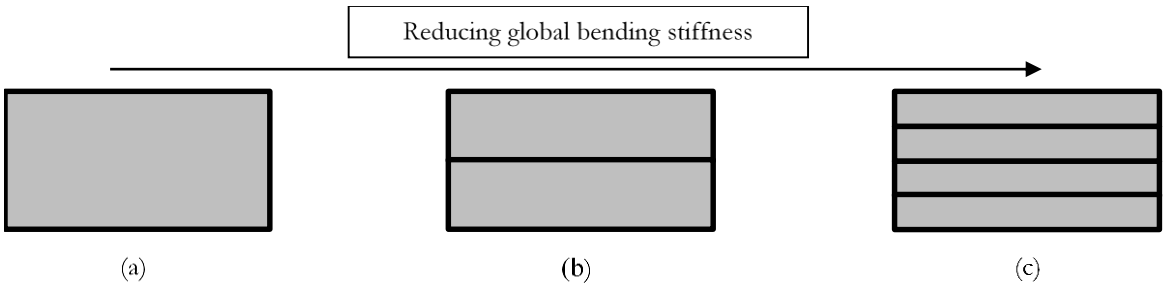

Figure 2: Beam configuration example (a) Solid (b) 2 elements (c) 4 elements

Whilst this variation is significant, this effect can be drastically enhanced via the use of sandwich structures [3]. By locating the split interface within a softer core material, the stiffness modulation between the split and electrostatically bonded configurations is far greater in principle.

2.3 Level of Adhesive Force

In order to effectively switch between the connected and unconnected configurations, the level of shear holding force at the interface is of vital importance. In existing research using this technology, the highest level achieved to date in this style of configuration was recorded at just below 0.1 MPa [2]. From earlier work by Di Lillo *et al.,* it is clear that, theoretically, much higher shear forces could be achieved, and thus the connection interface should be designed with the following in mind [10].

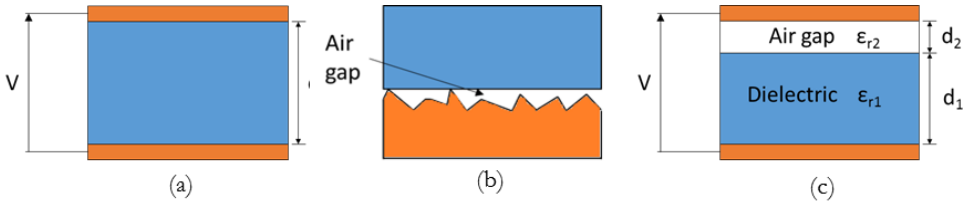

Figure 3: (a) Parallel plate configuration (b) Air gap from surface roughness (c) Parallel plate configuration with air gap

For the parallel plate electrode configuration shown in Figure 3 (a) the generated level of normal force from the application of a voltage U can be approximated using Equation 3. S is a geometric term for the contact area of the electrodes, and ε_0 is the permittivity of free space (8.854×10^{-12} Fm^{-1}). ε_r is the relative permittivity of the dielectric layer.

$$P_N = \frac{\varepsilon_0 \varepsilon_r U^2 S}{2d^2} \tag{3}$$

Localised surface roughness and lack of planarity can, however, introduce an air gap between contact surfaces (Figure 3 (b)) [7,11]. This air gap leads to greater separation of the plates than expected, and also introduces a region of lower permittivity (Figure 3 (c)). Thus, from the work of Mao *et al.* a better approximation for the expected level of holding force (for a given air gap) can be found [12].

$$P_N = \frac{\varepsilon_0 \varepsilon_{r1} \varepsilon_{r2}^2 U^2 S}{2(\varepsilon_{r1} d_2 + \varepsilon_{r2} d_1)^2} \tag{4}$$

It is assumed that the area *(S)* and the permittivity of free space *(ε_0)* are constants. In order to maximise the level of holding force, the potential difference *(U)* should be maximised, the dielectric thickness *(d_1)* should be minimised, and the relative permittivity of the dielectric *(ε_{r1})* should be optimised to the air gap thickness. The air gap *(d_2)* should be reduced to maximise the real contact area, and maximise the holding force. These factors were all considered when designing the composite integrated electrodes. Note that the force generated is a normal force, but the requirement is for shear stress transfer. The coefficient of friction (μ) is thus a multiplier for the above normal force to determine the shear force. This is later found in Section 5.3 as $\mu = 0.213 \pm 0.02$. Using an Electrostatic finite element model in COMSOL Multiphysics, the expected level of holding force of such an electrostatic adhesion device for a given geometry and applied voltage using Equation 4 can be verified. The finite element model and calculated values matched closely, with a suggested normal holding strength of 0.267 MPa at 4 kV with an example air gap of 2 μm. In reality, an air gap of 2 μm between the contact surfaces is unlikely, but is used here simply to demonstrate the close match between the analytical formula (Equation 4) and the electrostatic finite element model. An increase in the air gap would lead to lower holding force. The real surface variations may lead to discrepancies between the level of force observed and that estimated from Equation 4, even with a more representative air gap estimation.

Table 1: Equation 4 Value Comparisons

Example	Area (mm)	Air Gap (μm)	Voltage (kV)	Normal Force (N)		Strength (MPa)	
				COMSOL	Equation 4	Normal	Shear
1	4200	2	2	280.11	280.12	0.067	0.014
2	4200	2	3	630.26	630.28	0.150	0.032
3	4200	2	4	1120.46	1120.49	0.267	0.057

3 DESIGN AND FABRICATION

For this study a co-cure method developed in a previous study to integrate electrode devices into composite structures was used [11]. A thin film laminate of polyimide and copper provides the necessary electrodes for the application of electrostatic adhesion, whilst providing insulation from the host structure.

3.1 Fabrication Method

Samples were produced using a laminate of 35 μm electrodeposited copper on 25 μm polyimide (GTS Flexible Materials Ltd, UK). This material functions as the electrodes either side of the connection interface. For monolithic composite samples, the laminate material was co-cured along with carbon fibre reinforced polymer (CFRP) (SE70 carbon epoxy pre-preg tape, Gurit, UK). The CFRP laminates had a unidirectional (UD) layup (all 0°, parallel to the longitudinal direction of the beam in three-point bending) for simplicity of fabrication. For initial composite sandwich samples, 3 mm closed cell PVC foam (EasyCell75, EasyComposites, UK) was used as a core to which both the CFRP skins, and the electrodes were bonded. The method used an epoxy laminating resin (EL2 Epoxy, EasyComposites, UK) cured at ambient temperature under vacuum for 30 hours. During the bonding process, excess Copper-polyimide material was used, allowing the laminate to function as its own release film. This reduced the imperfections introduced to the external electrode surface during cure. Samples were cured against a polished aluminium tool plate, with the exception of Samples SA4 13 which were cured against polished glass. Alternative foams could further improve this initial finish. The copper surface was polished post-cure to further improve the surface finish.

(a) (b)

Figure 4: (a) Monolithic CFRP with integrated electrodes (b) Sandwich panel using GFRP skins and PVC foam core with integrated electrodes

For each configuration, the electrostatic adhesive interface is located on the centreline of the structure. The core material is used either side of this interface, thus the overall core thickness is that shown in Table 2.

3.2 Design to Maximise Holding Force

The chosen sample geometry is shown in Table 2 with reference to Figure 1. The geometry was selected to ensure that any variations in bending stiffness introduced by the electrostatic adhesion of the electrode were clearly observable.

Table 2: Test Samples' Geometry and Features

Feature		F1 Monolithic	C1 Core	C2 Core	SA4-12&13 Sandwich
Width (w)	[mm]	30	30	30	30
Length (l)	[mm]	150	150	150	150
Span (L)	[mm]	130	140	140	140
Skin Thickness (t_s)	[mm]	0.8	–	–	0.8

Core Thickness (t_c)	[mm]	0	6	6	6
Core Type	–	–	PVC Foam	PVC Foam	PVC Foam
Skin Type	–	CFRP	–	–	CFRP
Dielectric used	–	Mylar	Mylar	Hostaphan RNK	Mylar
Dielectric Thickness (d)	[mm]	23	23	12	23

The key design choice for maximising the achievable holding force is the choice of dielectric material. A polyester film (Du Pont Mylar A) was chosen as a suitable candidate due to its high dielectric strength (~4kV at 23 μm), allowing for the use of high voltages at relatively low thicknesses, properties desirable for this application (see Section 2.3). In addition to this, the relative permittivity of 3.2 and assumed friction coefficient of 0.5 were deemed acceptable. An alternative material, a polyethylene terephthalate (PET) film (Hostaphan RNK, Mitsubishi Plastics, JP) was found, suggesting improved properties compared to the Mylar film. With a dielectric strength of 4.2 kV at 12 μm and relative permittivity of 3.3, this film was selected for further testing. Samples C 1and C2 used the thin film electrodes mounted only to the core material, enabling an easily observable comparison between the dielectric options

Sample F1 considered using the electrodes mounted directly to the CFRP face sheets. Samples SA4-12 and 13 were produced as in Section 3.1.

3.3 Material Properties

Materials testing was carried out to assess the basic flexural properties of the constituent structural materials. The testing was performed in accordance with ATSM D790-10, using a three-point bend flexural configuration. An INSTRON 8433 test machine with a 1 kN load cell was used, and deflection measurements were taken using a video gauge extensometer. The average moduli of elasticity for the UD CFRP and PVC Foam calculated from the results were 104,827 ±5500 MPa and 66.5 MPa ±2.3 MPa respectively.

3.4 Theoretical Achievable Variation

Simple beam theory can be used to estimate the maximum achievable modulation between the "ON" and "OFF" configurations. Continuing from Section 2.2, we can represent the "OFF" configuration as two separate beams as in Figure 5 (a), each carrying half of the total load. For the "ON" configuration, the upper and lower beams would ideally be fully coupled, and thus behave as a single beam entity, as shown in Figure 5 (b). The theoretical flexural stiffness difference between the two configurations can thus be established.

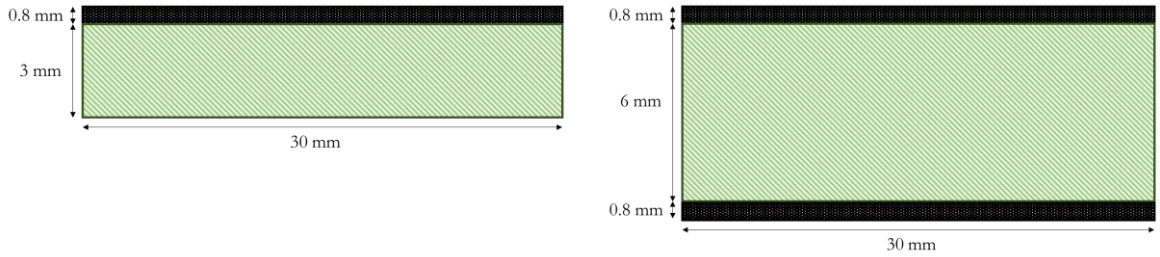

Figure 5: Cross sectional geometry (a) "OFF" Configuration, with each half carrying half the total load (b) "ON" Configuration, full load

Each configuration stiffness can be represented as an effective sectional bending stiffness EI_z. This value is calculated using Equation 5, where E_{xi} refers to the Young's Modulus of a component *i* of the section, and I_{zi} refers to the second moment of area of component *i*.

$$\overline{EI_z} = \sum E_{x_i} I_{z_i} \tag{5}$$

Thus Configuration (a) possesses an effective sectional bending stiffness of 320,444 Nmm² (2 sections of 160,222 Nmm²). The equivalent value for Configuration (b) is 58,470,673 Nmm². This represents 182.5 times increase in flexural stiffness. This topology change thus has great potential for large scale flexural stiffness modulation, provided that sufficient latching across the central interface is provided. In reality, the electrostatic attachment will not provide sufficient attachment to produce configuration (b), and, therefore, the observed stiffness will lie somewhere between the two calculated values.

4 EXPERIMENTAL SET-UP

4.1 Mechanical Testing

Table 2 shows the four test configurations. A three-point bend flexural test was used to obtain a load-displacement curve for each beam at a variety of applied voltages. A 1 kN load cell connected to an INSTRON 8433 test machine was used to apply the vertical loading at a rate of 10 mm/min up to 5 N for each monolithic sample and up to 20 N for each sandwich structure. Each sample was tested with five separate applied voltages: 0, 1, 2, 3 and 4 kV, with ten tests in total for each sample at each voltage. The load-displacement curves from each test can be used to observe the effect of the applied voltage on the global stiffness, and thus the ability of electroadhesive devices to modulate the stiffness.

4.2 Electrical Setup

A high voltage DC-DC step up convertor (commercially available EMCO *F Series*, EMCO High Voltage Corporation, USA) was used to impart a high voltage across the integrated electrodes. A potential divider was used as a means to measure the output voltage.

5 RESULTS

Three-point bend flexural tests were carried out to assess the operability of the electro-adhesive variable stiffness elements for a range of structural configurations and materials choices.

5.1 Monolithic Sample (Test F1)

Co-curing the copper-polyimide laminate with CFRP produced two thin composite plates with integrated electrode layers, insulated from the host structure. This configuration yielded a change in maximum deflection (at 5 N centre load) of -5.5% with the application of 4 kV across the electrostatic adhesive interface. Whilst this demonstrates a degree of variable stiffness functionality, the effect is limited by this structural configuration. Sandwich structures were thus investigated as a likely means to achieve a greater performance.

5.2 Foam Core Only (Tests C1 and C2)

PVC foam samples were tested without composite skins at this stage for rapid assessment of the operability of the electrostatic interface (Figure 6).

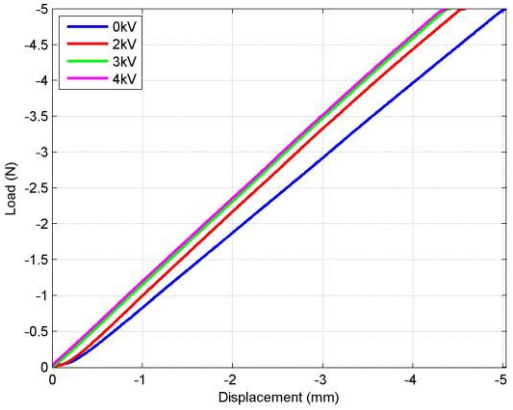

Figure 6: Load-displacement curves for foam core only three-point bend flexural tests (Sample C1)

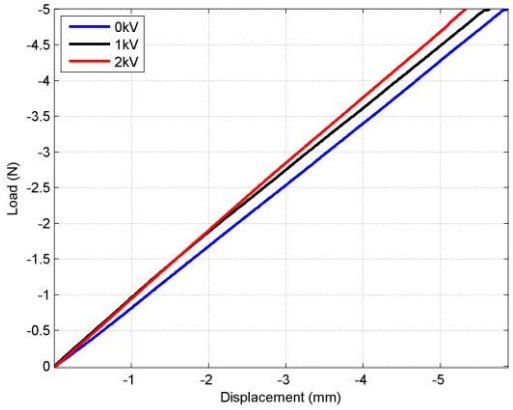

Figure 7: Load-displacement curves for foam core only three-point bend flexural tests using Hostaphan RNK dielectric film (Sample C2)

Note that despite being a monolithic structure as for sample F1, we now obtain a 13% decrease in the maximum deflection at 5 N loading for the 4 kV voltage for sample C1 (11.5% stiffness increase). This represents a promising initial result, and an even greater stiffness modulation might be achieved when such devices are integrated into a sandwich configuration. It is worth noting that even in the "OFF" configuration at 0 kV, the sample appears stiffer than expected from the calculations of Section 3.4. This is probably attributable to the additional stiffness of the resin layer. The primary interest of this study is the achievable stiffness modulation, and thus this is not hugely problematic at this stage. When designing for a specific stiffness, this shall be investigated further.

An alternate thin film dielectric material, Hostaphan RNK, was tested due to its promising quoted properties at a reduced available thickness of 12 μm. Upon the application of a 2 kV potential difference across the electrodes, a 9% reduction in maximum deflection is observed (Figure 7) (8.9% stiffness increase). This is a minor decrease compared

to the deflection reduction using the Mylar dielectric film, which is unexpected given the large reduction in dielectric thickness (see Section 2.3). It is, therefore, possible that the minimum electrode separation distance is limited by another feature in the configuration, such as improperly trimmed edges, or lack of planarity of the electrode faces. Other factors such as reduced friction coefficient or relative permittivity could also cause such reduction in effect.

Another feature of note is that initially the 1 kV and 2 kV load-displacement curves (Figure 7) appear similar but at around 2 N for the 1 kV there is a reduction in gradient, leading to a larger maximum displacement. This highlights that the holding force affects the stiffness profile in two ways. Firstly, a stronger holding force across the interface should lead to a steeper load-displacement curve, denoting a higher overall bending stiffness. The level of holding force generated will also determine the maximum shear stress that can transmitted via the interface. Above this value, a pseudo-plastic stick-slip failure mode is observed, hence a gradient reduction in the load-displacement curve (above a certain load), an effect referred to as "softening" by Bergamini *et al* [3]. Values could not be obtained for > 2 kV due to early dielectric breakdown of the Hostaphan RNK. Given the suggested dielectric strength of 4.2 kV, this was unexpected. Sharpness at the extremities of the electrodes could be the root cause of these early dielectric breakdowns, and thus in future, improved edge finishing would be beneficial.

5.3 Sandwich Structure Tests (SA4 1 and 2)

Samples SA4-12 and -13 represent composite sandwich structures with integrated electrostatic adhesive elements. Figure 8 shows the variation in load displacement curve achieved through the application of potential difference across the integrated electrodes. It is clear that the change in topology from a monolithic structure to sandwich beam structure facilitates more substantial flexural stiffness variations. Increased voltage leads to increased slope gradient, representing increased bending stiffness. This is an expected result, as the increased voltage should lead to increased holding force across the central interface, allowing for a larger shear force transfer between the adjacent surfaces, thus causing the beam to behave in a more coupled manner.

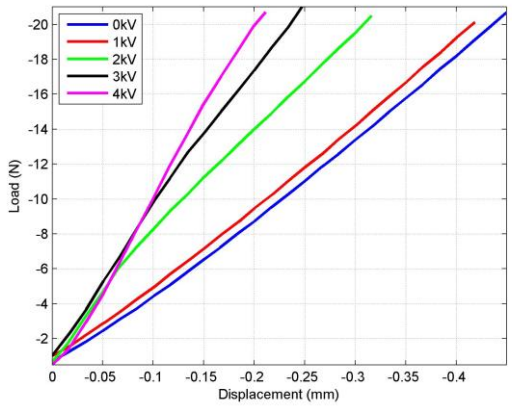

Figure 8: Load Displacement Curves for Composite Sandwich Structures with Integrated Electrostatic Adhesion (Sample SA4-12)

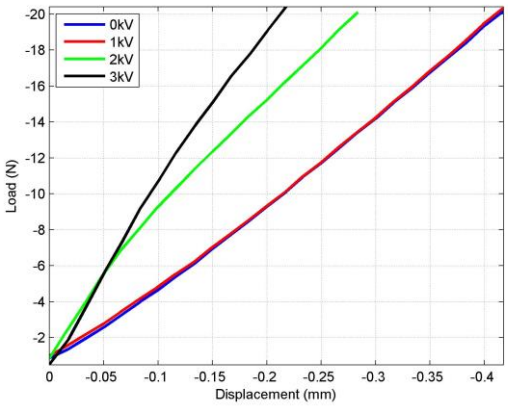

Figure 9: Load Displacement Curves for Composite Sandwich Structures with Integrated Electrostatic Adhesion cured against a Polished Glass Tool plate (Sample SA4-13)

This effect can be further increased through a minor alteration to the fabrication process. The use of a glass plate when bonding the electrode elements to the foam core can yield improvements to the electrode surface finish. From Figure 9 it can be seen that greater stiffness modulation can be achieved for a given voltage compared to Sample SA4-12.

In addition to the overall improved performance observed for sample SA4-13 compared to sample SA4-12, some other effects can be observed from Figure 9. Firstly, the effect of the application of a 1 kV potential difference across the interface seems minimal. Previous research suggests a minimum "turn-on" voltage before the electrostatic adhesion effect is observed, so to an extent this behaviour is expected [2]. It is possible that there is a certain degree of variability to the absolute voltage at which this occurs, originating from the DC/DC step up converter. Further investigation is required to confirm this hypothesis. The direct effect of the electrostatic adhesive coupling on the flexural stiffness of the beams can also be observed more clearly in Figure 9. Increased potential difference leads to an increase in the maximum stiffness, shown by steeper curve gradient for 3 kV compared to 2 kV, but also a less pronounced softening effect is observed (as referred to in Section 5.2). Using beam theory, an estimate for the maximum shear stress in the equivalent fully coupled sandwich beam (assuming perfect bonding) can be obtained [13]. This maximum value appears at the neutral axis of bending, and thus provides a useful comparison to the interfacial shear stress at the electroadhesive interface located at that neutral axis (for the "*ON*" configuration). Given that the core thickness (t_c) is sufficiently larger than the face sheet thickness (t_s), and the face sheets are significantly

stiffer than the core ($E_f >> E_c$), the flexural rigidity of the sandwich beam (D) can be simplified to Equation 6. Considering then a shear force per unit width of T_x, the maximum shear stress can be approximated using Equation 7.

$$D = \frac{E_f t_f d^2}{2} \tag{6}$$

$$\tau_{c,max} = \frac{T_x}{D}\left(\frac{E_f t_f d}{2} + \frac{E_c t_c^2}{8}\right) \tag{7}$$

From Figure 9 the softening effect appears to commence at around 5.5 N when applying 2 kV to SA4-13, and 9N for the 3 kV application. Equation 7 gives estimated shear stress at these loads to be 0.013 N/mm² and 0.022 N/mm² respectively. These values are close to the 0.011 N/mm² and 0.020 N/mm² shear strength values shown in Table 4. This thus increases confidence that the softening effect observed is directly influenced by the level of electrostatic adhesion.

The improved performance of the glass cured sample SA4-13 compared to the standard sample SA4-12 can be seen in Figure 10. The stiffness values (K) were calculated using Equation 10, found from manipulating the basic flexural deflection formula for the bending configuration tested. The slope values used the curve sections between 1 and 20 N to account for any initial non-linearity. It is acknowledged that this slope values are not fully representative of the load-displacement curves, as the softening effect leads to a gradient reduction above a given load for each curve. For the chosen loading window, the use of the slope of the linear approximation was deemed an acceptable means of comparison between each configuration.

$$\delta = \frac{PL^3}{48EI} = \frac{PL^3}{48K} \tag{8}$$

Where P is the applied load, L is the support span, E is the equivalent isotropic Young's Modulus, I is the Second Moment of Area, δ is the deflection at the central span load position and K is the equivalent flexural stiffness. For each curve with a linear relationship, assuming zero deflection at zero load for each curve:

$$P = \alpha\delta \tag{9}$$

Where α represents the approximated gradient of each curve. Hence from Equations 8 and 9 we can determine:

$$K = \frac{\alpha L^3}{48} \tag{10}$$

For Figure 10, trend lines were not included as the operation of the devices at higher voltage is yet to be established. There will be an upper limit of the level of achievable holding force for a given device, which can be found from Equation 4. Table 3 displays the achieved percentage stiffness variation for both of the sandwich configurations.

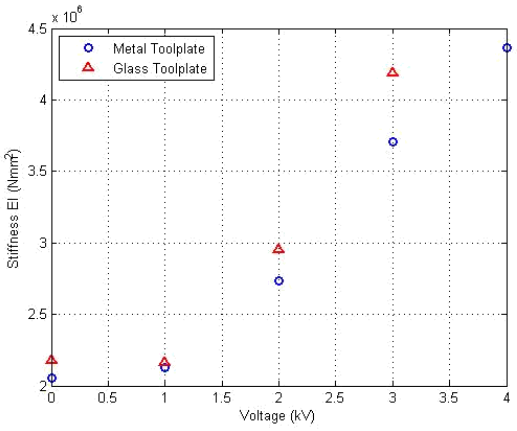

Figure 10: Effect of Electrostatic Adhesive Voltage on Sandwich Flexural Stiffness

Table 3: Percentage Stiffness Modulation

Voltage		Percentage Change in Flexural Stiffness SA4-12	SA4-13
0	[kV]	0%	0%
1	[kV]	4%	-1%
2	[kV]	33%	36%
3	[kV]	80%	93%
4	[kV]	112%	-

Whilst substantial, these changes are significantly smaller than the theoretical modulation suggested in Section 3.4. The holding force strength generated was thus investigated. Using a shear test rig with a 2 kg sled mass, Sample SA4-13 was established to have a friction coefficient of 0.213 ± 0.02 and average shear holding forces as in Table 4. The values refer to the change in shear holding force compared to the 0 kV average of 4.17 N ± 0.30 N (10 tests).

Table 4: Electrostatic Shear Force Tests

Voltage		Average Maximum Electrostatic Shear Force		Average Maximum Electrostatic Shear Strength		Eq. 4 Expected Electrostatic Shear Force (d_2=3.5 μm)	
1	[kV]	2.91 ± 0.49	[N]	0.0007	[MPa]	10.95	[N]
2	[kV]	45.40 ± 8.84	[N]	0.011	[MPa]	43.79	[N]
3	[kV]	84.79 ± 10.56	[N]	0.020	[MPa]	98.54	[N]

The holding forces shown in Table 4 are lower than those suggested in Table 1. The expected shear holding force for an air gap of 3.5 μm is provided for comparison. The differences observed in terms of the trend of these results is likely due to the assumption that the interface topology can be simplified to Figure 3 (c). Given the difficulty in fabrication of two perfectly planar sandwich panels, and the open cell nature of the core material, some areas will likely have much higher separation than others, which could provide an initiation location for interface failure. The 1 kV value is far lower than expected, but does however support the reasoning that minimal stiffness variation was observed due to a lack of electroadhesive holding force generated across the interface. The strengths seen are also lower than the 0.1 MPa quoted in the work of Di Lillo *et al* [2]. Those tests considered a double lap shear joint of thin film materials. The double lap joint doubles the available holding force for a given sample width, at a given voltage, compared to the single lap joint present in samples used here, and the thin film materials have a greater conformability to allow for close electrode contact. The stiff nature of the sandwich beams fabricated in this study restricts the motion of the electrodes, likely limiting the real contact area between adjacent electrodes, thus restricting the holding force.

The observed strengths are also lower than the maximum estimated shear stress in the core material for this beam configuration (0.028 MPa), and significantly lower than the shear strength of virgin PVC core (1.09 MPa). The reduced stiffness compared to the theoretical maximum (for a sandwich beam with solid foam core) is therefore understandable behaviour, as the shear stress transfer between the upper and lower sections is severely limited. As the achievable holding force is increased, the resistance to sliding between the layers is increased, yielding higher stiffness. The limited strength of the electrostatic interface in comparison to the core strength however restricts the "ON" configuration from behaving like the idealised sandwich beam Figure 5 (b).

5.4 Surface Contact Considerations

The air gap value of 3.5 μm used for the comparisons in Table 4 was selected as it provided a close match to the observed electrostatic shear forces from testing. Assessments of the surface topography of the electrode surfaces were carried out using an optical 3D micro-coordinate system (InfiniteFocus, Alicona Ltd, UK) to establish the validity of assuming such a surface separation. Whilst it was not possible to capture the complete electrode surface due to limits on the data processing power, representative areas could be captured by considering the variations across the width and length of one electrode of sample SA4-13 independently. Across the width of the sample, for the 2.15 cm test length considered, the observed variation in surface profile height was very low, with an average waviness of the profile at 2.3 μm. It was noted however that larger surface separation may occur for the when considering variations along the length of the sample, as any warping of the beam would more likely occur about this primary bending axis. Figure 11 shows the primary profile for a strip along the length of the electrode surface. Whilst this shows a larger separation, the shape gives light to why this is less of a concern, as only a light force (~0.5N) applied to perpendicular to the electrode surface, would lead to global bending sufficient to close such a gap.

The surface separation once the electrodes are brought in to close contact are thus dependent on surface roughness and waviness of the local profile. Removing the primary curvature of the profile, the roughness and waviness

parameters for a profile length of 8 cm were as shown in Table 5. From this data it can be seen that with two similar electrode surfaces, the separation introduced from the surface variations should be close to the 3.5 µm estimate. This low roughness and low waviness finish is a result of the integration of the electrode elements through a cold-cure bonding process using a highly planar tool plate. The close contact between adjacent surfaces that this permits contributes significantly to the high levels of holding strength achieved.

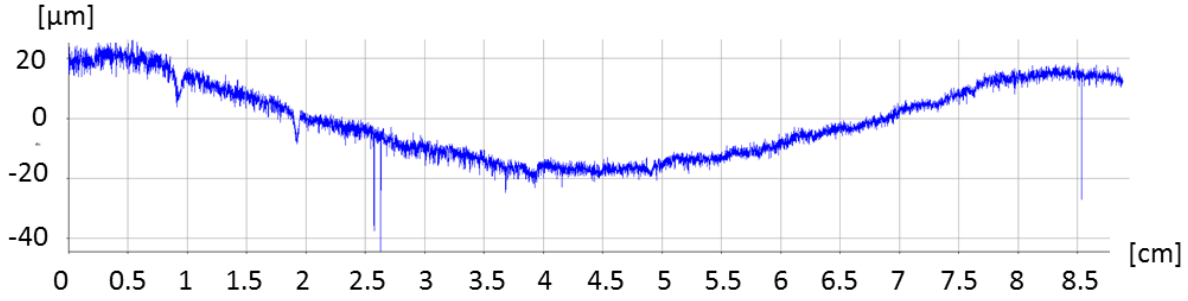

Figure 11: Profile of Sample SA4-13 electrode surface over 8 cm longitudinal profile

Table 5: Surface Profile Data for Sample SA4-13 Electrode

Name	Description	Value	Unit
R_a	Average roughness of profile	0.76	[µm]
R_q	Root-Mean-Squared roughness of profile	1.08	[µm]
W_a	Average waviness of profile	1.18	[µm]
W_q	Root-Mean-Squared waviness of profile	1.41	[µm]
P_a	Average height of profile	1.63	[µm]
P_q	Root-Mean-Squared height of profile	2.15	[µm]
P_{sk}	Skewness of height profile	-1.33	

Larger air gaps will exist at the visible defects on the electrode faces, although all of those observed have been found to be depressions in the electrode surfaces (Figure 12). Whilst such defects lead to a localised increase in the included air gap, they do not cause larger scale bridging, and are thus far less significant than an equivalent sized protuberance. The negative skewness of the height profile further confirms that the larger variations are recesses in the surface profile.

Figure 12: Height Map of a Visible Electrode Surface Defect

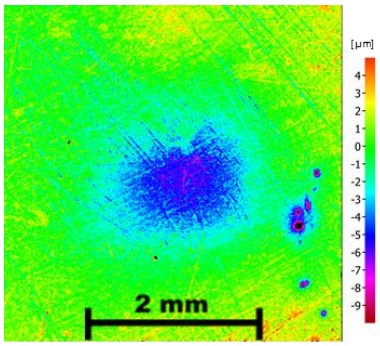

6 CONCLUSIONS

In this study, electrostatically modulated variable stiffness functionality of composite sandwich structures has been demonstrated. Through application of a 4 kV potential difference across the integrated electrodes, a 112% stiffness increase was achieved in a CFRP skinned PVC core composite sandwich panel. The use of a copper polyimide laminate thin film material allows for the inclusion of low profile electrode elements that are insulated from the host structure. The fabrication method for such incorporated devices is relatively simple when compared to the lamination and cure cycle required for standard FRP composite sandwich panel production. Improvements to the surface finish of the integrated electrodes enabled a further 13% increase in the achieved stiffness value at 3kV compared to the standard finished device.

The integrated electrostatic adhesive elements have demonstrated the ability to vary the stiffness of the host structure at higher loads than existing devices. This variable stiffness capability at higher loading conditions increases the potential applications for such functional structures. Further stiffness modulation could be achieved through increased electrostatic holding force across the dielectric interface, in order to further increase the shear stress transfer between electrostatically bonded sections. Dielectric improvements, namely relative permittivity and dielectric strength, are key to achieving these enhancements. Such improvements could help to eliminate early dielectric breakdowns that have prevented further sample testing at 4 kV in this study. The improved performance achieved from electrode surface enhancement highlights the requirement for close surface contact between the electrodes. Developments to facilitate enhanced contact could further increase the variable stiffness capability of this technology.

ACKNOWLEDGEMENTS

The authors wish to acknowledge Mr. Mark Fitzgerald for his assistance with the electrical rig design and safety testing. Many thanks to the James Dyson Foundation for funding this research.
This research was in part presented at ICCM 20 Copenhagen 19-24th July 2015.

REFERENCES

[1] Gibson R F 2010 A review of recent research on mechanics of multifunctional composite materials and structures *Composite Structures* **92** 2793–810

[2] Di Lillo L, Raither W, Bergamini A, Zündel M and Ermanni P 2013 Tuning the mechanical behaviour of structural elements by electric fields *Applied Physics Letters* **102** 224106

[3] Bergamini A, Christen R, Maag B and Motavalli M 2006 A sandwich beam with electrostatically tunable bending stiffness *Smart Materials and Structures* **15** 678–86

[4] Kuder I K, Arrieta A F, Raither W E and Ermanni P 2013 Variable stiffness material and structural concepts for morphing applications *Progress in Aerospace Sciences* **63** 33–55

[5] Tabata O, Konishi S, Cusin P, Ito Y, Kawai F, Hirai S and Kawamura S Microfabricated tunable bending stiffness device *Proceedings IEEE Thirteenth Annual International Conference on Micro Electro Mechanical Systems (Cat. No.00CH36308)* 23–7

[6] Bergamini A, Christen R and Motavalli M 2007 Electrostatically tunable bending stiffness in a GFRP–CFRP composite beam *Smart Materials and Structures* **16** 575–82

[7] Bergamini A 2009 *Electrostatic modification of the bending stiffness of adaptive structures* (ETH)

[8] Raither W, Bergamini a. and Ermanni P 2012 Profile beams with adaptive bending-twist coupling by adjustable shear centre location *Journal of Intelligent Material Systems and Structures* **24** 334–46

[9] Raither W, Simoni L De and Lillo L Di 2014 Adaptive-Twist Airfoil Based on Electrostatic Stiffness Variation *AIAA SciTech*

[10] Di Lillo L, Carnelli D a, Bergamini a, Busato S and Ermanni P 2011 Quasi-static electric properties of insulating polymers at a high voltage for electro-bonded laminates *Smart Materials and Structures* **20** 057002

[11] Heath C J C, Bond I P and Potter K D 2015 Integrating electrostatic adhesion to composite structures *SPIE 9433, Industrial and Commercial Applications of Smart Structures Technologies 2015* vol 9433 (San Diego) p 94330D

[12] Mao J, Qin L and Wang Y 2014 Modeling and simulation of electrostatic attraction force for climbing robots on the conductive wall material *2014 IEEE International Conference on Mechatronics and Automation (ICMA)* (IEEE) pp 987–92

[13] Zenkert D 1997 *An Introduction to Sandwich Construction* (Engineering materials advisory services)